Revista Mexicana de Astronomía y Astrofísica, **35**, 123–133 (1999)

3D TRANSFER OF THE DIFFUSE IONIZING RADIATION IN ISM FLOWS AND THE PREIONIZATION OF A HERBIG-HARO WORKING SURFACE

A. C. Raga,[1] G. Mellema,[2] S. J. Arthur,[1] L. Binette,[1] P. Ferruit,[3] and W. Steffen[4]

Received 1999 May 7; accepted 1999 June 17

RESUMEN

Hemos desarrollado un nuevo código tridimensional de dinámica de gases radiativos, que incluye un tratamiento de la radiación ionizante difusa producida en el flujo. Describimos este código en detalle, y luego lo aplicamos al problema de la preionización en la superficie de trabajo de un jet Herbig-Haro (HH).

Esta simulación numérica muestra la estructura espacial del precursor de una superficie de trabajo de un jet HH. Como ha sido previamente descrito en el contexto de choques plano paralelos, la radiación difusa ioniza y calienta el flujo prechoque. Encontramos que la radiación ionizante difusa también modifica en forma significativa la estratificación del flujo post-choque y la localización de los choques, probablemente resultando en distintos espectros producidos por los modelos con y sin radiación difusa. Mapas de la emisión Hα calculados de nuestras simulaciones muestran que la zona preionizada será difícil de observar, debido a su falta de brillo comparado con el de la zona poschoque del choque de proa.

ABSTRACT

We have developed a new 3D radiation-gasdynamic code which includes a treatment of the transfer of the diffuse ionizing radiation produced by the flow. We describe this code in some detail, and then apply it to the problem of preionization in the working surface of a Herbig-Haro (HH) jet.

This 3D numerical simulation shows the spatial structure of the precursor of a working surface of a HH jet. As has been previously described in the context of plane-parallel shocks, the diffuse radiation both ionizes and heats the preshock flow. We find that the diffuse, ionizing radiation also significantly affects the post-shock flow stratification and the location of the shocks in the simulations, likely leading to different predicted spectra for models with or without diffuse radiation. Synthetic Hα emission-line maps produced from our simulations show that the preionized region will be difficult to observe due to its faintness compared to the post-bow shock emitting region.

Key words: **HYDRODYNAMICS — ISM: JETS AND OUTFLOWS — SHOCK WAVES**

1. INTRODUCTION

The problem of preionization in plane-parallel shocks in the ISM has been treated in some detail in the past. Following the original paper of Shull & McKee (1979), it has become standard to include a treatment of the radiative precursor in steady, plane-parallel shock models. Such a treatment has also been included in time-dependent, plane shock models (Innes, Giddings, & Falle 1987a, b).

Interestingly, the stratification and the observational properties of the preionized region in plane-parallel shocks of Herbig-Haro (HH) objects has rarely been discussed. The situation is different in the field of active galactic nuclei, where it has re-

[1] Instituto de Astronomía, Universidad Nacional Autónoma de México.
[2] Stockholm Observatory, Sweden.
[3] Department of Astronomy, University of Maryland, U.S.A.
[4] Instituto de Astronomía y Meteorología, Universidad de Guadalajara, México.

cently been proposed that radiative precursors could have a strong contribution to the observed emission line spectrum (Dopita & Sutherland 1995; Morse, Raymond, & Wilson 1996), and detailed predictions of the spatial stratification and observational properties of radiative precursors have been made (Dopita & Sutherland 1995, 1996).

Considerably less attention has been directed to the problem of preionization in non-plane parallel flow configurations. The principal paper in this subject is the one of Raymond, Hartigan, & Hartmann (1988). These authors have computed an approximate radiative transfer for the preionized region upstream of a bow shock. They have modeled the bow shock in the 3/2D approximation of "short postshock cooling distances" (Hartmann & Raymond 1984; Raga & Böhm 1985) and used their estimates of the ionizing flux produced by the postbow shock region to compute the preionization fraction as a function of position along the bow shock. For a discussion of the approximations used in this calculation, we refer the reader to the paper of Raymond et al. (1988). Unfortunately, these authors do not discuss the spatial stratification and the observational properties of the preionized region upstream of a bow shock.

Raga & Wang (1994) present a much simpler, fully analytic "Strömgren region" approach for treating the problem of preionization in a bow shock formed in a shocked cloudlet flow. These authors do attempt to carry out predictions of the spatial structure of the radiative precursor. However, their "Strömgren region" approach is hampered by the fact that the thickness of the ionization front is comparable to the physical size of HH objects and their preionized regions.

In the present paper we present a 3D gasdynamic simulation of the working surface of an HH jet, which includes a treatment of the transfer of the diffuse, ionizing field produced by the postshock region. As far as we are aware, this is the first time that such a simulation is attempted.

In the majority of the previous 3D gasdynamic simulations, the computations have been conducted whithout radiative transfer, commonly using the 'on the spot' approximation, in which one assumes that the produced ionizing radiation is reabsorbed locally. A few simulations of flows, including the radiative transfer of ionizing radiation, have been conducted in the past (e.g., Raga et al. 1997; Mellema et al. 1998), but they were limited to the much simpler case of the transfer of the radiation from a central source. They did not include the problem of the transfer of the diffuse radiation, which in principle requires the computation of how the radiation produced at each point in the grid influences all the other positions.

In situations in which the diffuse field dominates over the ionizing field from a central source, like the case of the working surface of an HH jet, the "on the spot" approximation breaks down and appropriate handling of the transfer of the diffuse radiation becomes critical. We have therefore developed a new 3D numerical code, including the calculation of the effect of the diffuse field within a hydrodynamic simulation, and we have used this code to simulate the working surface of a HH jet. As far as we are aware, this is the first time that such a simulation is conducted.

The layout of the paper is as follows. Section 2 describes our numerical method, § 3 describes the results for the case of the preionization by a fast jet, and § 4 sums up the conclusions.

2. NUMERICAL METHOD

2.1. *Gasdynamics*

The gasdynamic equations are numerically integrated on a three-dimensional, uniform, Cartesian grid. The continuity equation, the three momentum equations, the energy equation (including the energy gain by photoionization, and the energy loss by emission of radiation and by collisional ionization), and a continuity equation for neutral hydrogen (with the appropriate source term, see § 2.2) are solved. The "flux vector splitting" algorithm of Van Leer (1982) has been used, extended to second order spatial accuracy by introducing linear gradients within the cells (as described by Arthur 1991). We have used this algorithm quite extensively in the past to carry out two-dimensional (Cartesian and cylindrically symmetric) simulations of diverse flows (see, e.g., Raga & Noriega-Crespo 1998).

2.2. *Atomic Physics*

In order to keep the program as simple and fast as possible, we have chosen a simplified form for dealing with the microphysics of the gas. We solve for the ionization and heating/cooling using operator splitting, which means that in each timestep the calculation is done separately from the hydrodynamic calculation. This independent ionization and heating/cooling timestep only affects the H I continuity equation and the energy equation.

It would of course be possible to include the ionization and heating/cooling together with the hydrodynamic timestep. We have tried doing this, and carried out comparisons with the calculations with the operator splitting (described above), finding almost identical solutions with the two approaches. For our larger simulations we therefore use the operator splitting approach, which appreciably shortens the computational time.

We assume that the gas is 90% hydrogen and 10% helium, with a small abundance of singly ionized carbon (10^{-4}, by number) to keep the electron density

from going to zero in cool regions. For the hydrogen gas we solve the time dependent ionization and cooling, taking into account radiative recombination, collisional ionization, and photo-ionization by the diffuse field. We assume that helium is at most singly ionized, and that the ionization of He I follows the one of H I. We then calculate the electron density as $n_e = n_{C\,II} + n_{H\,II} + n_{He\,II}$.

We should note that the assumption of having at most singly ionized helium is, of course, incorrect for the high velocity bow shocks of the simulations that we have computed. The effects of this incorrect assumption, however, are probably masked by the errors introduced by the rather low resolution of our calculations, and by the fact that we use a simple cooling function, which does not include many of the relevant processes in a proper way (see below).

Since only a small part of the grid contributes strongly to the diffuse field we have chosen the radiative recombination coefficient to be case B, and we describe its temperature dependence with a power law of index -0.79 (see Cantó et al. 1998). For the collisional ionization we use the coefficients of Cox (1970). The method used to solve the transfer of the diffuse, photo-ionizing field is described in the next section.

In order to solve the rate equation describing the ionization of hydrogen, we assume that the temperature and density are constant within each timestep, and that the electrons come from H and He or from singly ionized C. With these assumptions, it is possible to integrate the rate equation analytically to obtain the H neutral fraction at the end of the timestep. This method was used in the original plane-parallel shock models of Cox (1970).

For the thermal properties of the gas we take into account the radiative cooling (Λ) and the heating (Γ) due to photoionization by the diffuse field. The cooling is calculated with the prescription described by Biro (1994) and Biro, Raga, & Cantó (1995), which includes cooling due to collisionally excited H Ly-α, [O I] and [O II] lines (the ionization state of oxygen being assumed to follow the ionization state of H), as well as collisional ionization and radiative recombination of H, and a switch to a parametrized cooling function at high temperatures. The radiative heating rate includes the heating due to Lyman continuum photons (following the approximate treatment of Cantó et al. 1998) and to the He II λ305 line. Actually, we multiply the contribution of this line by a factor 2 in order to bring the diffuse flux up to values comparable to the ones obtained with calculations in which other UV emission lines are included. The same processes are included in the calculation of the photoionization rates.

2.3. *Diffuse Radiation*

To deal with the transfer of the diffuse radiation we use a version of what is known as the "method of short characteristics". In this method one derives the column density from a source point to a destination point using neighbouring points. A more accurate method would be to do the transfer directly from the source point to the destination point (known as the "method of long characteristics"), but on a three dimensional grid this would be impractical in view of the very long computation time which is necessary. An alternative approach is used by Razoumov & Scott (1999), who do not compute the transfer between all points, but only use a limited number of rays and interpolate between them. Both the short characterics and the limited ray tracing methods suffer from a certain amount of diffusion because of the interpolation. However, with a limited number of rays one can easily miss strongly emitting and/or absorbing points, and we have therefore chosen the short characteristics method. A two dimensional version of this was already used in Raga et al. (1997) and Mellema et al. (1998), for treating the direct radiation from a central source.

Our implementation in three dimensions works as follows. We step through the grid, identifying the stronger source points. Once we find a source point $S(x_s, y_s, z_s)$, we calculate the column density from it to all other grid points. For this, we step through the three dimensional grid in planes of constant z, starting at $z = z_s$. We calculate the values for the entire plane and then move on to the next plane. For each point, the interpolation works as shown in Figure 1. For a point $P(x_i, y_j, z_k)$ we calculate the position of the point C where a direct ray from the source $S(x_s, y_s, z_s)$ cuts through the cube of which P is a corner point. Point C can lie on any of the six planes of the cube depending on the position of the source (S) with respect to P. In Fig. 1 we show the situation in which C lies on the z_{k-1} plane, the solution for the other 5 cases being analogous. In this case $C(x_c, y_c, z_{k-1})$.

We derive the column density N_C and neutral hydrogen density $n_{0,C}$ at point C by performing a (possibly weighted) average between the four corner points in the z_{k-1} plane, using their distances to C to determine the weights. Because of the order in which we step through the grid, these densities and column densities were determined earlier. We also calculate the path length l from C to P and then find the column density at point P as

$$N_P = N_C + l\, n_{0,C}\,. \qquad (1)$$

This method is simple, and does not require a lot of storage space (a major concern when doing three dimensional calculations).

In order to test the method we calculated the column densities on a 100^3 grid for a source point located at point (0,0,50). The grid is filled with a uni-

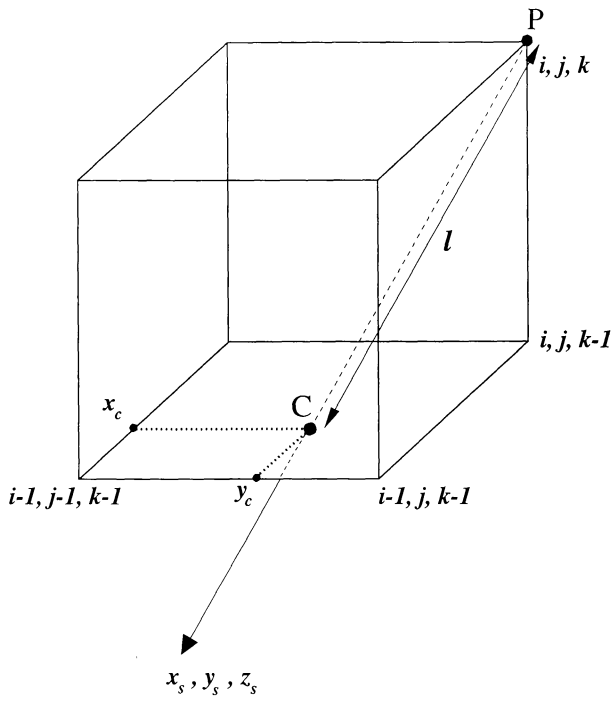

Fig. 1. Geometry for the radiation transfer of the diffuse field. The figure shows one grid cell in the three dimensional grid. The ray from source point (x_s, y_s, z_s) to (x_i, y_j, z_k) crosses the z_{k-1} plane at x_c, y_c. The distance from this crossing point to (x_i, y_j, z_k) is l.

form density $n = 1$, except for a spherical region of radius 20, centred at (50,50,50) which has a $n_s = 10$ density. We also calculated the analytic solution for the column density for this configuration.

Figure 2 shows contour plots of the column density in four planes of constant z comparing the numerical (dashed) and analytic (solid) solution. One sees that the two match quite well, except near the edges of the "shadow region", where the numerical method overestimates the column density. The diffusion of the numerical method spreads the shadow region by about 10 grid cells. We experimented by weighting the interpolation with the inverse of the density and column density so that lower densities are favoured. This leads to less spreading but a worse fit for the column densities inside the sphere. We have chosen to carry out our simulations with an unweighted interpolation between the computational grid points when carrying out the integration of the radiative transfer.

2.4. *The Numerical Simulation*

With the gasdynamic+radiative transfer code described above, we have computed a numerical simulation of the working surface of a radiative, HH jet. We have computed a model for a neutral jet of initial radius $r_j = 10^{16}$ cm, velocity $v_j = 267$ km s^{-1}, density $n_j = 225$ cm^{-3} and temperature $T_j = 1000$ K, moving into an also neutral environment of density $n_e = 25$ cm^{-3} and temperature $T_e = 1000$ K (C is assumed to be singly ionized in both the jet and the environment). The computational domain has $80 \times 80 \times 80$ grid points, with a uniform grid spacing of 7×10^{14} cm in the three dimensions.

We start the simulation with a jet moving along the z-axis, with a beam extending over one-half of the domain. In order to keep the working surface at the same position, we give the beam a velocity of 67 km s^{-1} in the +z direction, and the environment a velocity of -200 km s^{-1} (the sum of which gives the $v_j = 267$ km s^{-1} jet velocity of our model). It is straightforward to verify that the two velocities (given to the jet and to the environment) satisfy the standard ram-pressure balance condition required for the working surface to remain stationary in the computational grid. This kind of numerical setup has been previously used by Raga et al. (1995).

We should note that a bow shock velocity of 200 km s^{-1} (resulting from our choice of jet velocity and jet-to-environment density ratio, see above) is consistent with the velocities deduced from the emission line widths of the higher excitation HH objects, such as HH 32 (see, e.g., Solf et al. 1986). The line widths HH 80/81 (which probably is the highest excitation HH object) imply even larger bow shock velocities (Heathcote et al. 1998).

We have carried out two simulations:

- the first simulation includes the transfer of the diffuse ionizing radiation. In order to keep the simulation from being exceedingly slow, we have only considered the ionizing radiation emitted by the grid points with emission coefficients larger than 10% of the peak value of the emission coefficient (at the time in which the radiative transfer is computed). This choice results in the computation of the radiation emitted by 2000 to 5000 grid points (this number changes as the time integration progresses).
- In the second simulation, the transfer of the ionizing radiation has not been computed.

We should note that we have tested the effect of changing the cutoff in the emission coefficient of the ionizing radiation. The region emitting the ionizing radiation is strongly concentrated to the stagnation region of the bow shock, and the emission coefficient has a very steep decrease towards the bow shock wings. Because of this, we find that very similar flow structures are obtained when using different cutoff values for the emission coefficient (we have carried out tests with the cutoff value ranging from 30% down to 5% of the peak value of the emission coefficient in lower resolution simulations).

Some of the results obtained from these simulations are shown in Figure 3. This figure shows the temperature, density and neutral hydrogen fraction

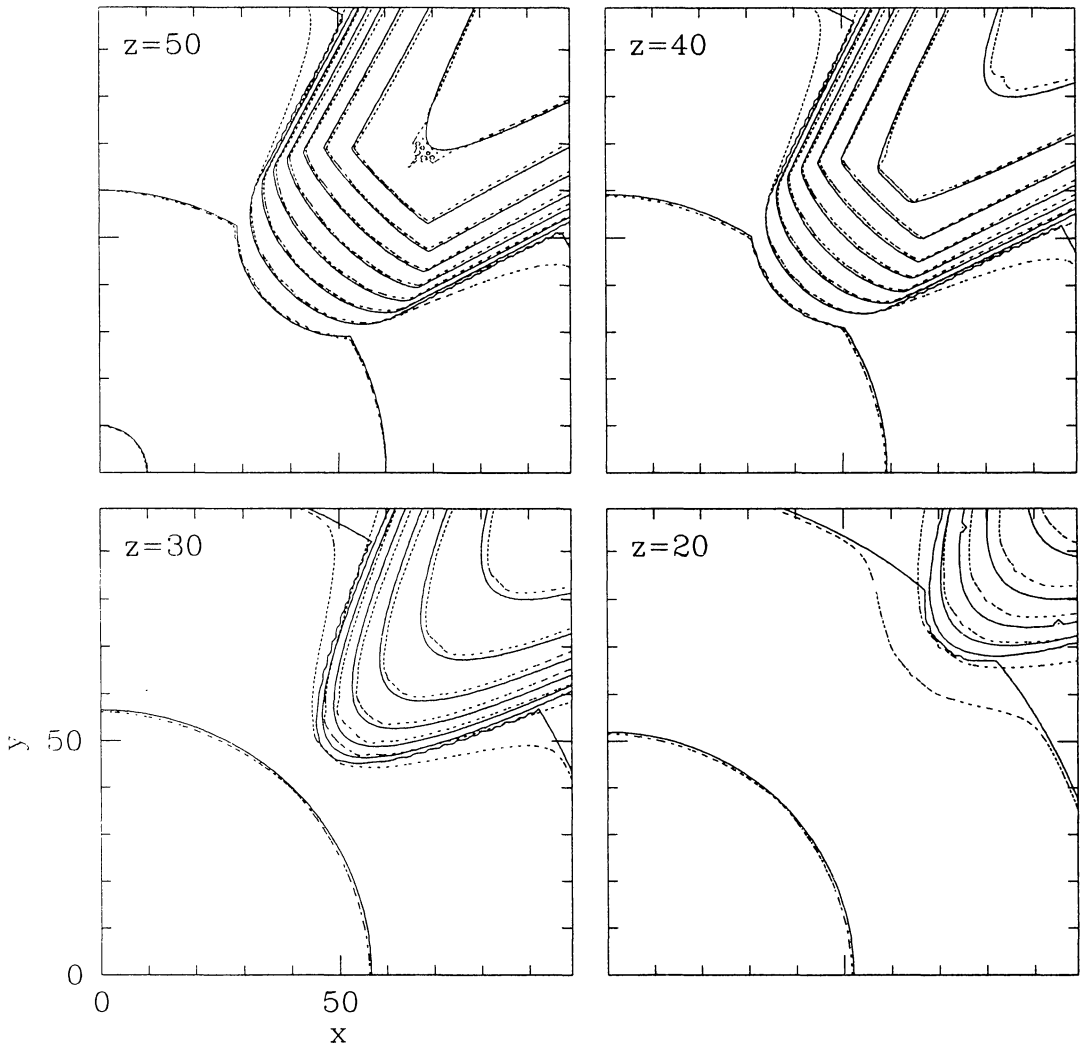

Fig. 2. Contour plots for the column density to the point (0,0,50) on a 100^3 grid containing a high density sphere of radius 20 centred at (50,50,50). The plots show the column density in the planes $z = 50$, 40, 30, and 20, with contours representing linear steps of 50. The solid contours correspond to the analytic solution, and the dashed contours to the numerical solution.

stratifications obtained after a $t = 100$ yr time integration for the models with and without transfer of the diffuse, ionizing radiation. The contour plots represent the stratification in the xz-plane. In the model with radiative transfer, the presence of the radiative precursor can be clearly seen. This precursor is spatially extended, having a characteristic size of about twice the jet diameter. We should note that the conspicuously flat-topped bow shocks that we obtain are typical of radiative jets with square ("top hat") density and velocity cross sections (see the discussion of Raga et al. 1998).

Figure 4 shows temperature, density (of atoms and ions) and neutral hydrogen fraction cuts along the z-axis obtained from the two models. In the model with radiative transfer we see that the gas is preheated to temperature of $\sim 4 \times 10^4$ K and that the neutral hydrogen fraction reaches a value of ~ 0.02 directly before the shock (the corresponding values for the simulation without the diffuse field being a temperature of 1000 K and a hydrogen neutral fraction of 1). The density perturbations due to the presence of the radiative precursor are very small. Figure 5 shows cuts parallel to the x-axis at a postition $z = -10^{16}$ cm and $y = 0$ (see Fig. 3). In the immediate preshock region, the temperature has a value of $\sim 1.5 \times 10^4$ K and the neutral hydrogen fraction is ~ 0.5.

From Figures 4 and 5, it is clear that the differences between the models with or without ionizing

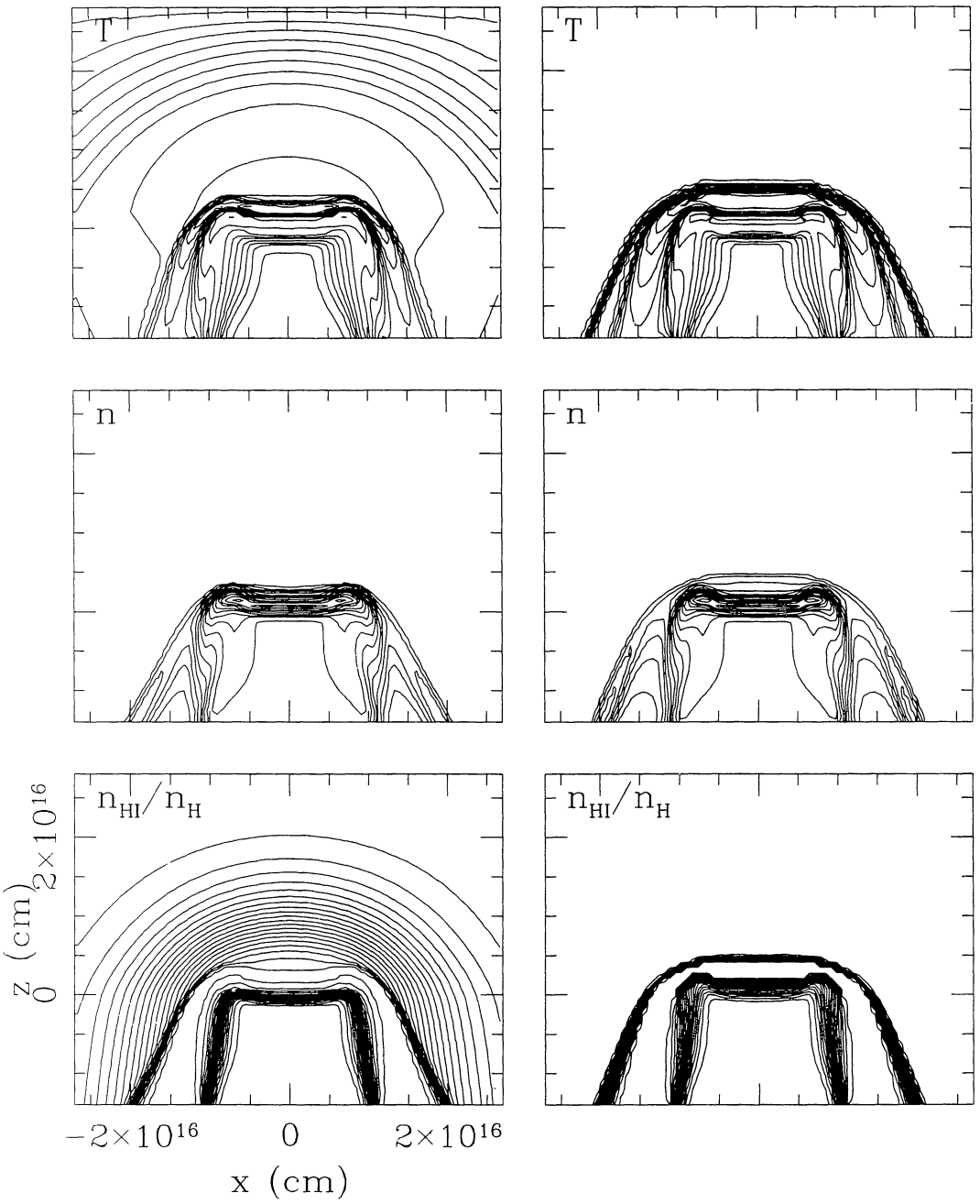

Fig. 3. Temperature (top), ion+atom number density (centre) and neutral hydrogen fraction (bottom) obtained after a $t = 100$ yr time integration for the working surface models with (left) and without (right) transfer of the diffuse, ionizing radiation (see the text). The environment flows in the $-z$ direction so that the working surface always remains close to the origin of the coordinate system. The temperature and density stratifications are depicted with logarithmic, factor of 2 contours. The neutral hydrogen fraction is depicted with linear contours starting at a value of 0.99, and descending in linear steps of 0.05.

radiation transport are not restricted to the presence (or absence) of the radiative precursor. The stratifications of the shocked regions as well as the precise position of the shocks are also different. Even though our models do not include the different atomic/ionic species necessary for carrying out detailed predictions of the emission line spectrum, it is clear that the different stratifications will lead to different predicted spectra for the two models.

Some of the differences between the models with or without ionizing radiation transport can be understood in a simple way. For example, from Fig. 4 we

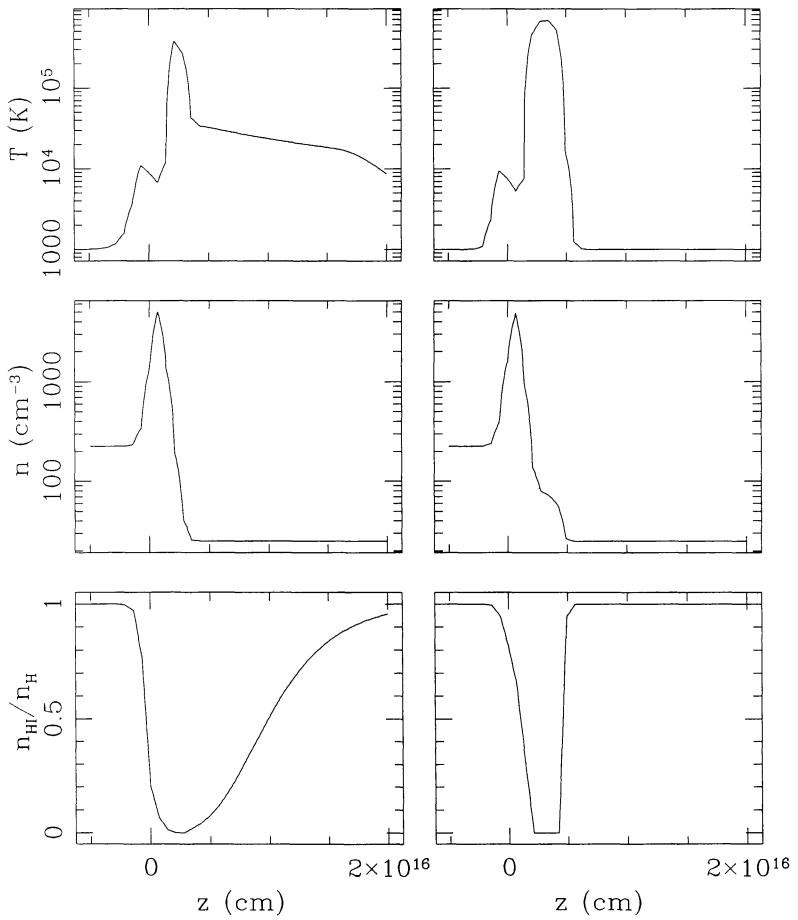

Fig. 4. Temperature, density (of atoms and ions) and neutral hydrogen fraction cuts along the z-axis (i.e., along the $x = 0$, $y = 0$ line) obtained from the two models described in the text (also see Fig. 3).

see that the stagnation region post-bow shock temperature is lower in the simulation with the diffuse, ionizing field. This result is somewhat unintuitive, since one would naively expect that the higher preshock temperature of this simulation would lead to a somewhat higher post-shock temperature. Interestingly, for a bow shock velocity of 200 km s^{-1} (i.e., for a Mach number well in excess of 10), the preshock temperature has a negligible effect on the jump conditions. Also, the energy loss due to collisional ionization of hydrogen (which would tend to produce a lower temperature for the simulation with neutral pre-shock material) is negligible for a 200 km s^{-1} shock. The effect that we see in our simulation is the direct result from the shock jump conditions that the temperature behind a strong shock is a factor of 2 higher if the number of particles per unit mass grows by a factor of 2 in going through the shock (i.e., the situation found in the simulation without diffuse field) compared to the case with no change in the number of particles per unit mass (i.e., the situation found in the simulation with diffuse field).

In Figure 6 we show the local shock velocity, and the immediate preshock temperature and neutral hydrogen fraction of the bow shock as a function of cylindrical radius (given in units of the radius r_j of the jet) obtained from the model with radiative transfer. In this figure, the shock velocity and the hydrogen ionization fraction are directly compared with the results obtained by Raymond et al. (1988) for a 200 km s^{-1} bow shock of parametrized shape.

Given the differences in the approaches used by us and by Raymond et al. (1988), the agreement between the two models is reasonably good. In particular, the different dependencies of the shock velocity versus cylindrical radius are due to the fact that while Raymond et al. (1988) assume a smooth, curved shape for the bow shock, the bow shock resulting from our simulation has a rather flat, on-axis region. Due to this different bow shock shape, it is not surprising that the shape of the neutral hydrogen fraction versus cylindrical radius curve shows appreciable differences between the two models.

Finally, in Figure 7 we present predictions of the

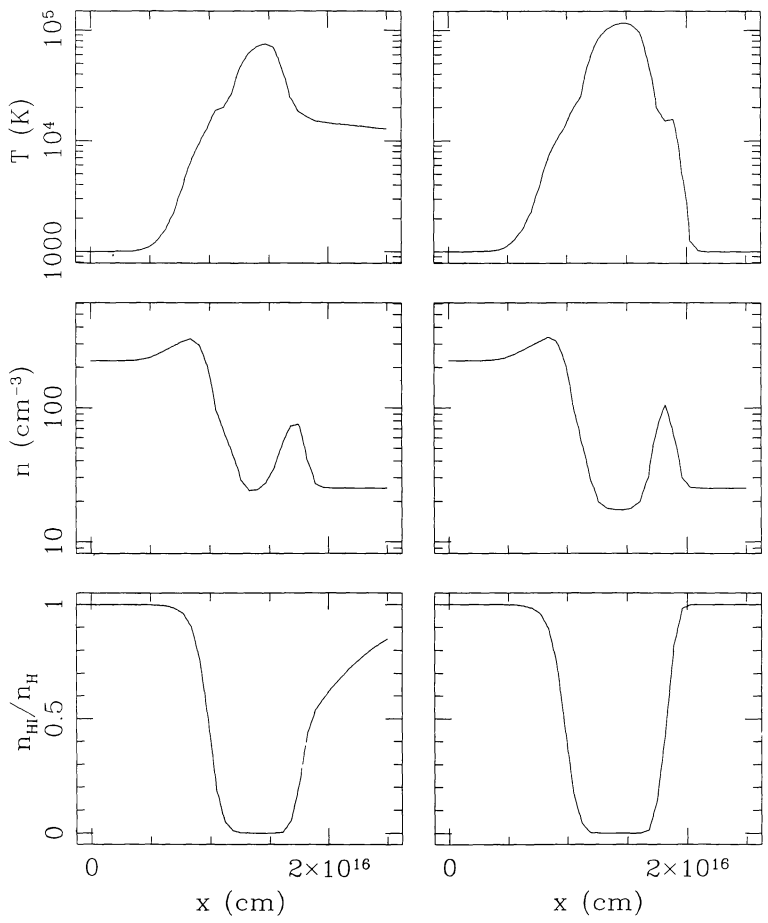

Fig. 5. Temperature, density (of atoms and ions) and neutral hydrogen fraction cuts parallel to the x-axis at a postition $z = -10^{16}$ cm and $y = 0$ (see Fig. 3) obtained from the two models described in the text.

Hα intensity maps from our models with and without radiative transport (assuming that the xz-plane is parallel to the plane of the sky). The main difference between the two maps is of course the presence (or absence) of the radiative precursor. Also, the post-bow shock emission presents partially different characteristics for the two models.

In order to evaluate whether or not it would be possible to directly observe the radiative precursor, we note that its Hα surface brightness is approximately 4 orders of magnitude fainter than the peak brightness of the working surface. The spatially integrated emission of the precursor is approximately 3 orders of magnitude fainter than the emission integrated over the postshock region. This huge contrast between the emissions of the postshock region and the precursor indicate that an extremely high signal-to-noise ratio would be neccesary in order to be able to detect the precursor observationally.

We should note that the Hα intensity map of the model without radiative transport (lower graph of Fig. 7) presents some numerical noise in the stagnation region of the bow shock. This numerical noise is the result of the fact that the calculations are carried out in single precision, which results in appreciable errors in the neutral fraction of hydrogen when the gas is almost fully ionized. As in the calculation of the Hα emissivity we include the effect of collisional excitation of neutrals to the $n = 3$ level of hydrogen, these errors show up as noise in the Hα intensity map. This numerical effect, however, is seen only in regions of the Hα map with intensities lower than the peak value by 5 to 6 orders of magnitude.

3. CONCLUSIONS

We have developed a new 3D gasdynamic+radiative transfer code, which includes the transfer of the diffuse, ionizing radiation. This code also follows the non-equilibrium ionization state of hydrogen. The

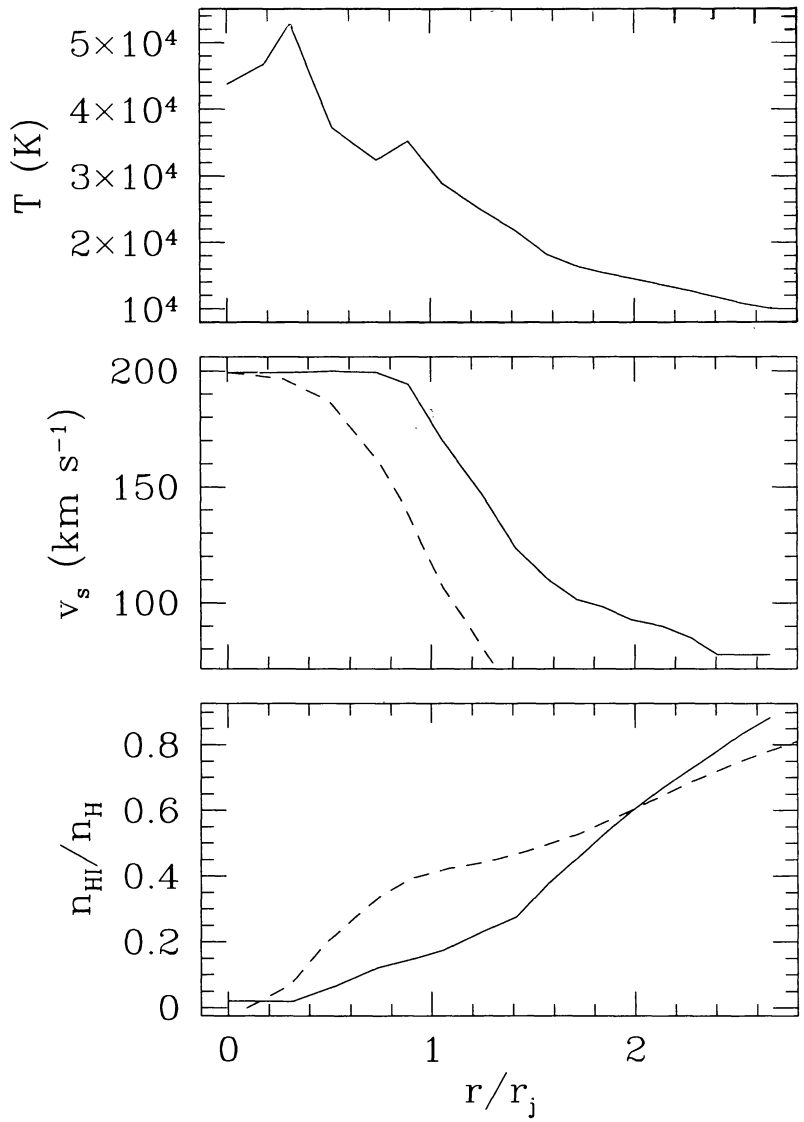

Fig. 6. The local shock velocity (centre), and the immediate preshock temperature (top) and neutral hydrogen fraction (bottom) of the bow shock as a function of cylindrical radius (or distance from the z-axis, given in units of the radius r_j of the jet) obtained from the model with radiative transfer (see the text). The results from our model are shown with solid lines, and the dashed lines show the results obtained by Raymond et al. (1988) for a 200 km s^{-1} bow shock.

radiative transfer is solved with a method that considers the points with large emission coefficients as independent sources, and the column densities from these points to all other grid points are computed.

We apply this code to the problem of preionization in the working surface of an HH jet. We have calculated working surface models with and without the transfer of the diffuse, ionizing radiation. From these models we illustrate the differences in the post-shock region introduced by the presence of a radiative precursor. However, we are not able to carry out predictions of the effects on the emitted spectrum, since our simulations do not include a treatment of the relevant atoms and ions.

We have computed Hα emission maps, which show the spatial distribution of the emission of the radiative precursor. We find that the emission integrated over the precursor is $\sim$ 3 orders of magnitude fainter than the emission from the postshock region. This result implies that it will be necessary to obtain very high signal to noise ratio observations in order to detect the emission from the precursor in an HH jet.

A question that is not resolved with our simulations is whether or not the precursor could be easier

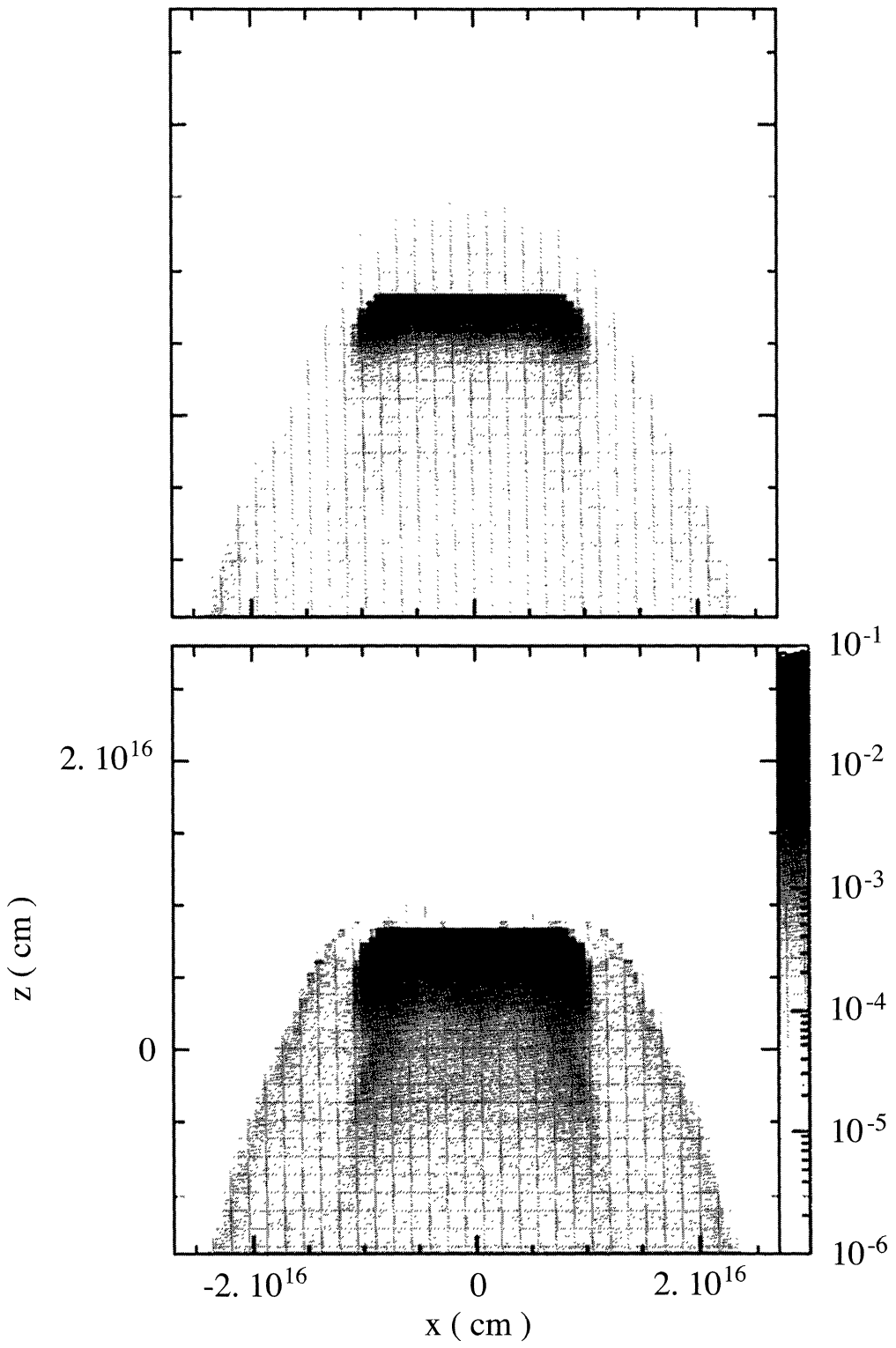

Fig. 7. Hα maps predicted from the models with (top) and without (bottom) transfer of the diffuse, ionizing radiation, after a time integration of $t = 100$ yr. It has been assumed that the xz-plane is parallel to the plane of the sky. The greyscale depicts the logarithm of the Hα intensity (normalized to the peak intensity).

to detect in some other emission lines. The fact that this region is partially ionized and is quite warm (in excess of 10^4 K) suggests that it might emit quite strongly in forbidden lines of neutral and/or singly ionized species. In order to answer this question, it will be necessary to carry out future numerical simulations including atoms and ions of elements (such as C, N, O and S) which produce strong forbidden lines.

In the future, we plan to extend the number of species and processes considered in the code, which will enable us to explore the effect of preionization in more energetic jets (e.g., in jets from Seyfert galaxies), where the observable effects of the preionization region are predicted to be much stronger.

We thank Sam Falle (the referee) for helpful comments about this paper. The work of L. Binette and A. Raga was supported by the CONACyT 26833-E grant. S. J. Arthur acknowledges support from CONACyT grant 25470-E.

REFERENCES

Arthur, S. J., Ph.D. thesis, University of Leeds
Biro, S. 1994, Ph.D. thesis, University of Manchester
Biro, S., Raga, A. C., & Cantó, J. 1995, MNRAS, 275, 557
Cantó, J., Raga, A. C., Steffen, W., & Shapiro, P. 1998, ApJ, 502, 695
Cox, D. P. 1970, Ph.D. thesis, University of California, San Diego
Dopita, M. A., & Sutherland, R. S. 1995, ApJ, 455, 468
_____. 1996, ApJS, 102, 161
Hartmann, L., & Raymond, J. C. 1984, ApJ, 276, 560
Heathcote, S., Reipurth, B., & Raga, A. C. 1998, AJ, 116, 1940
Innes, D. E., Giddings, J. R., & Falle, S. A. E. G. 1987a, MNRAS, 226, 671
_____. 1987b, MNRAS, 227, 1021
Mellema, G., Raga, A. C., Cantó, J., Lundqvist, P., Balick, B., Steffen, W., & Noriega-Crespo, A. 1998, A&A 331, 335
Morse, J. A., Raymond, J. C., & Wilson, A. S. 1996, PASP, 108, 426
Raga, A. C., & Böhm, K. H. 1985, ApJS, 58, 201
Raga, A. C., Cantó, J., & Cabrit, S. 1997, A&A, 332, 714
Raga, A. C., & Noriega-Crespo, A. 1998, AJ, 116, 2943
Raga, A. C., Noriega-Crespo, A., Steffen, W., Van Buren, D., Mellema, G., & Lundvist, P. 1997, RevMexAA, 33, 73
Raga, A. C., Taylor, S. D., Cabrit, S., & Biro, S. 1995, A&A, 296, 833
Raga, A. C., & Wang, L. 1994, MNRAS, 268, 354
Raymond, J. C., Hartigan, P., & Hartmann, L. 1988, ApJ, 326, 323
Razoumov, A. O., & Scott, D. 1999, MNRAS, in press
Shull, J. M., & McKee, C. F. 1979, ApJ, 227, 131
Solf, J., Böhm, K. H., & Raga, A. C. 1986, ApJ, 305, 795
Van Leer, B. 1982, ICASE report No. 82-30

Sarah Jane Arthur: Instituto de Astronomía, UNAM, Unidad Morelia, J. J. Tablada 1006, Col. Lomas de Santa María, Morelia, Michoacán, 58090 México (jane@astrosmo.unam.mx).
Luc Binette and Alex C. Raga: Instituto de Astronomía, UNAM, Apartado Postal 70-264, 04510 México, D.F., México (binette, raga@astroscu.unam.mx).
Pierre Ferruit: Department of Astronomy, University of Maryland, College Park, MD 20742, U.S.A. (pierre@blazar.astro.umd.edu).
Garrelt Mellema: Stockholm Observatory, SE-133 36, Saltsjöbaden, Sweden (garrelt@astro.su.se).
Wolfgang Steffen: Instituto de Astronomía y Meteorología, Universidad de Guadalajara, Ave. Vallarta 2602, 44130 Guadalajara, Jalisco, México. (wsteffen@udgserv.cencar.udg.mx).